



Traveling wave fault location for AC transmission lines: an approach based on the application of EMD and Teager energy operator

Andressa Oliveira¹ · Fernando Moreira² · Alessandra Picanço³ · Felipe Vasconcellos²

Received: 25 April 2024 / Accepted: 31 July 2024

© The Author(s), under exclusive licence to Springer-Verlag GmbH Germany, part of Springer Nature 2024

Abstract

This paper proposes an approach for the single-ended and the double-ended traveling wave-based fault location algorithm using the empirical mode decomposition associated with the Teager energy operator to extract characteristic data from the faulted voltage signals of an overhead transmission line. The simulation of the power system uses the JMarti line model, with an ideally transposed transmission line, and it was carried out using the alternative transients program (ATP) software. Subsequently, the MATLAB[®] software was used for extracting the traveling wave arrival times and to perform the single-ended and the double-ended fault location algorithms for all simulated scenarios in ATP. The numerical and graphical results prove that the proposed methodology with the Teager energy operator and the double-ended analysis can better extract the characteristic data of the voltage signals and estimate the fault location with good accuracy, with percentage error of 0.034% for the best results, depending only on the fault type and the sampling rate adopted.

Keywords Empirical mode decomposition · Fault location · Teager energy operator · Transmission line · Signal processing

Abbreviations

AC	Alternating current
ATP	Alternative transients program
DE	Double ended
DEEMD	Double-ended empirical mode decomposition

DEEMDT	Double-ended empirical mode decomposition with Teager energy operator
EMD	Empirical mode decomposition
IMF	Intrinsic mode function
FL	Fault location
SE	Single ended
SEEMD	Single-ended empirical mode decomposition
SEEMDT	Single-ended empirical mode decomposition with Teager energy operator
R_F	Fault resistance
SNR	Signal-to-noise ratio
TEO	Teager energy operator
TL	Transmission line
TW	Traveling wave

Fernando Moreira, Alessandra Picanço and Felipe Vasconcellos contributed equally to this work.

✉ Andressa Oliveira
andressa.poliveira@ufob.edu.br

Fernando Moreira
moreiraf@ufba.br

Alessandra Picanço
alepicanco@ifba.edu.br

Felipe Vasconcellos
felipe.vasconcellos@ufba.br

¹ Collegiate of Electrical Engineering, Federal University of Western Bahia, Av. Dr. Manoel Novaes, Bom Jesus da Lapa 47600-000, BA, Brazil

² Department of Electrical and Computer Engineering, Federal University of Bahia, Prof. Aristides Novis, 02, Salvador 40210-630, BA, Brazil

³ Department of Electrical Engineering, Federal Institute of Education, Science and Technology of Bahia, Emídio dos Santos, Salvador 40301-015, BA, Brazil

1 Introduction

Fault location (FL) is a challenging problem in the electric power system due to the vast extension of the electric power transmission lines (TLs). It requires precise identification of the occurrence and protection action of the affected section, with the goal of restoring the power supply as fast as possible.

The development of fault location methods in overhead systems has been investigated for many decades [1]. Cur-

rent efforts are focused on developing intelligent protection systems capable of accurately detecting, classifying, and locating faults. Fault location methods can be categorized into 3 main classes: circuit theory, traveling wave (TW) techniques, and artificial intelligence applications [2, 3].

The methods based on circuit theory require the sampling of nodal voltages and line currents at line terminals. The impedance measurement method is expressed in the frequency domain, and the fault distance is estimated based on the impedance value calculated using primary current and voltage data or current and voltage phasors. The main disadvantage of these methods is that their success depends on the characteristics of the transmission lines and is influenced by the value of the fault resistance [4].

The methods based on traveling wave theory indicate that the electromagnetic wave generated following a fault in a transmission line (TL) can be separated into a voltage wave, produced by the electric field, and a current wave, associated with the magnetic field. These generated voltage and current waves propagate in both directions along the line from the fault occurrence. The precise fault location depends on both initial instants of the transients and on the determination of the wave speed in the transmission line. The main disadvantages of traveling wave-based fault location methods are the difficulties in distinguishing between traveling waves reflected from the fault and those reflected from the remote end of the line, the requirement of a high sampling rate, and the higher implementation costs compared to impedance-based techniques [5].

The methods based on artificial intelligence applications employ various approaches including expert systems, fuzzy logic, and artificial neural networks. They are typically applicable when multiple data inputs are available. The demand for utilizing artificial intelligence (AI) algorithms has been increasing among researchers in recent years including in the field of fault location in power systems. References [6, 7], and [8] study the wavelet transforms and neural network (WNN), the traveling wave frequencies and extreme learning machine (ELM), and the convolutional adversarial neural network (CANN), respectively, for detection, classification, and fault location in power systems. The main disadvantages of methods based on artificial intelligence applications are the significant computational demands for training and processing, often requiring specialized high-speed microprocessors, and the fact that data collection process may require an extensive communication system with high bandwidth to gather synchronized information on a central server [4].

This paper presents an accuracy analysis from the application of the empirical mode decomposition (EMD) technique associated with the Teager energy operator (TEO) for the extraction of characteristic data from voltage signals in TLs based on traveling wave single-ended and double-ended FL [9]. The voltage signals are used in this application because,

during the fault, the voltage transient signal changes are more severe than the current signals [10].

The application of the EMD technique for the extraction of characteristic data was motivated because the signals under analysis are non-stationary and because the characteristics of this technique presented a better resolution to identify the exact moment of the sudden change in the frequency of the signal. Using the TEO associated with EMD allows highlighting the identification of variations in the magnitude and frequency of the signal with high computational efficiency and accuracy in identifying the TW arrival times [11, 12]. Single-ended (SE) and double-ended (DE) analyses were used to compare the efficiency of the applied identification methodology. Besides, the single-ended algorithm presents some peculiarities when compared to the algorithm with data from double-ended, its implementation cost is low, and it makes use of signals recorded at just one line terminal and does not require means of communication or even data synchronization [10, 13, 14].

Usually, in the analysis of fault location methods, the following situations should be considered: variation in the FL, the fault incidence angle, and different fault resistances (R_F). Reference [15] used classical EMD for the identification of the arrival time of the traveling wave from a single-phase fault in a power system, which can be precisely detected by the instantaneous amplitude. Reference [16] demonstrates the extraction of data features using EMD and the classification of faults employing a probabilistic neural network. Reference [11] illustrates the utilization of DEMD (down-sampling empirical mode decomposition) combined with the TEO for fault detection in distribution systems with radial and ring topologies. This approach ensures feasibility for real-time applications due to low computational complexity and immunity to data synchronization errors. The main contributions of the work here presented are shown in Table 1 comparing them with the literature: using EMD associated with TEO (EMDT) for an alternating current transmission line, using the JMarti line model, therefore considering the variation in the line parameters with frequency. The results are compared with the standard approaches for the EMD to prove the influence of the TEO on accuracy. As far as the authors know, the EMD technique associated with TEO has not been applied for this type of study yet, which consists of an approach for the single-ended and the double-ended traveling wave-based FL for an alternating current transmission line with different sampling rate values and the influence of the signal-to-noise ratio (SNR).

The text is organized as follows: Sects. 2 and 3 show the empirical mode decomposition and Teager energy operator, respectively. Section 4 presents the application of the technique (EMD with TEO) for extracting data characteristics for FL in the TL. Section 5 presents the case study adopted for the analysis and discussion developed. Section 6 presents the

Table 1 Contributions presented in this work

Subject	Literature	This work
Fault detection	Downsampling EMD with TEO for electrical distribution system [11]. EMD with probabilistic neural network [16]	Simple threshold is outlined with the aerial mode of the current signals
Fault classification		
Fault location	Classic EMD data extraction in TL with TW [15]	EMD with TEO data extraction in TL with TW

study of the sensitivity analysis variables for the approaches applied in single-ended and double-ended scenarios: fault resistances, incidence angles, fault types, sampling frequencies, SNRs, and computational cost. Finally, the conclusions of this work are presented in Sect. 7.

2 Empirical mode decomposition

The Hilbert–Huang transform developed in [17] is a very applicable analysis method for non-stationary signals and uses empirical mode decomposition, which does not admit an analytical definition and decompose non-stationary signals into intrinsic mode functions (IMF) [18].

The decomposition of the signal into a finite, usually small, number of intrinsic mode functions is part of the Hilbert–Huang transform. It allows the identification of parameters inherent to the signal, such as the variations in amplitudes and frequencies. The process of extracting IMFs is called sifting [17–19].

After decomposition, the Hilbert transform is applied to the chosen IMF to obtain the instantaneous frequency of the data. When the signal is decomposed into a series of IMFs $c_i(t)$, its corresponding Hilbert transform [$H_i(t)$] is defined by [15, 18]

$$H_i(t) = \frac{1}{\pi} \int_{-\infty}^{+\infty} \frac{c_i(\tau)}{t - \tau} d\tau \tag{1}$$

The final results are an energy–time–frequency distribution, which is called the Hilbert spectrum [17]. Thus, an analytical signal $Z_i(t)$ can be formed by

$$Z_i(t) = c_i(t) + jH_i(t) = a_i(t)e^{j\Theta_i(t)} \tag{2}$$

where $a_i(t)$ is the instantaneous amplitude and $\theta_i(t)$ is the instantaneous phase defined as

$$a_i(t) = [c_i(t)^2 + H_i(t)^2]^{\frac{1}{2}} \tag{3}$$

$$\Theta_i(t) = \arctan\left(\frac{H_i(t)}{c_i(t)}\right) \tag{4}$$

The instantaneous frequency $f_i(t)$ of $c_i(t)$ is given by

$$f_i(t) = \frac{1}{2\pi} \frac{d\Theta_i(t)}{dt} \tag{5}$$

3 Teager energy operator

The Teager energy operator is a nonlinear operator with the advantages of high accuracy in signal demodulation and high processing speed in addition to quickly identifying the instantaneous energy of the signal and efficiently detecting any abrupt variation in the signal [12].

Reference [20] defined TEO in the discrete and continuous time domains as a tool for analyzing signal components from the energy point of view. For signals in the continuous time domain, it can be defined by

$$\Psi[x(t)] = \left(\frac{dx(t)}{dt}\right)^2 - x(t)\frac{d^2x(t)}{dt^2} \tag{6}$$

where Ψ is the TEO and x is the signal in the continuous time-domain. The corresponding operator for the discrete time-domain signal is given by

$$\Psi[f(n)] = f^2(n) - f(n+1)f(n-1) \tag{7}$$

Graphically analyzing the energy values with such an application, the first peak corresponds to the moment when the wave arrives for its detection.

4 Application of EMDT for fault location

4.1 Test system studied

The test system studied, shown in Fig. 1, consists of a 360 km long TL, with ground resistivity of 100 Ωm, operating at 50 Hz, between 2 Thevenin equivalents representing large areas with energy supply. The illustration shows a single-phase fault (AG) applied at $t = 0.045$ s (when the switch closes). The fault is eliminated at 0.1 s (when the switch opens).

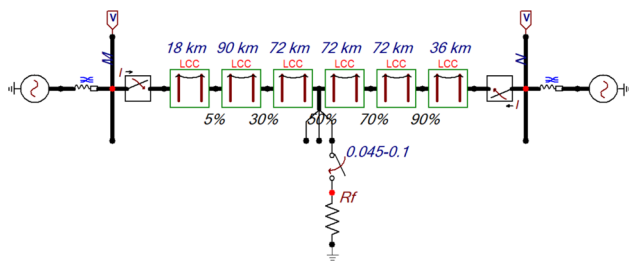


Fig. 1 Test system for the study of fault location

Table 2 Proposed system parameters

Parameters	Thevenin equivalents	
	Terminal M	Terminal N
Source voltage	400k $V_{L-L,20^\circ}$	400k $V_{L-L,0^\circ}$
Z_{s1}	$(2 + j1.5) \Omega$	$(2 + j1.5) \Omega$

Table 3 Line conductor characteristics

	Type	Diameter (mm)	Resistance DC (Ω/km)
Phase conductors	Cardinal	30.35	0.0586
Shield wire	7N8	9.78	1.4625

The system’s transmission line was characterized by utilizing frequency-dependent distributed parameters, aiming to create a more realistic model for the AC transmission line systems. The complete transmission line consists of five line sections, allowing the electrical power system simulation with different FLs along the line. The details of the sources and the transmission line are presented in Tables 2 and 3, and in Fig. 2 [21].

4.2 Considerations adopted in the analysis

For the analysis of the test system, the current and voltage signals were obtained at both terminals (M and N), as identified in Fig. 1. The effects of the main parameters that may affect the single-ended and the double-ended FL accuracy are analyzed in this study through the voltage signals, as shown in Table 4, such as the variation in the fault resistance, the incidence angle, the sampling rate, and the FL (distance from the local terminal) for all fault types (where A, B, and C are the phases and G is the ground).

Noise refers to undesired electrical signals, commonly characterized by a broad spectrum typically below 200 kHz, and they are superimposed on the power system voltage or current in phase conductors. The typical noise magnitude is less than 1% of the voltage magnitude [22]. To show the influence of noise on the proposed algorithm, white Gaussian noise is added to the voltage and current signals to produce a specified signal-to-noise ratio (SNR). Different SNR val-

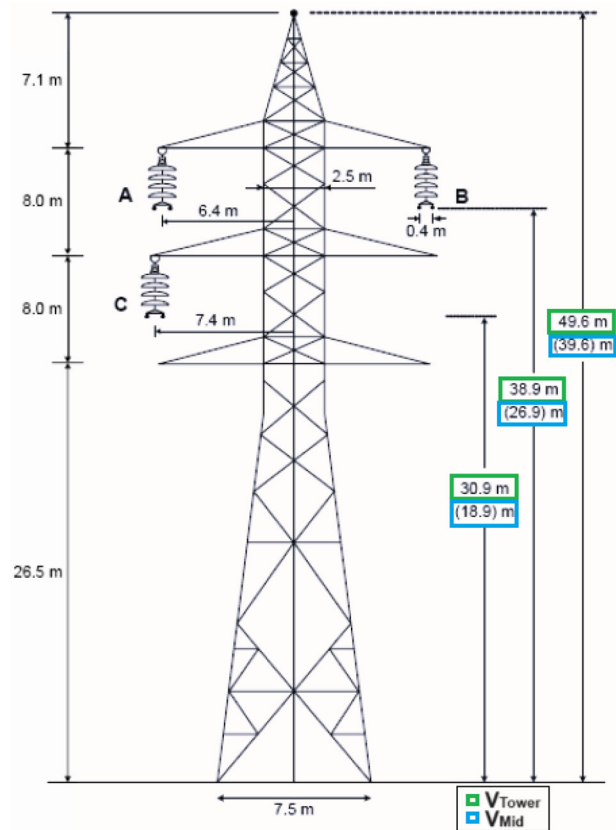


Fig. 2 Phase configuration of transmission line and tower size

Table 4 Fault simulation variables used in the analysis

Simulation variables	Values
Fault location (km)	18, 108, 180, 252, 324
Fault type	AG, BG, CG, ABG, BCG, ACG, AB, BC, AC, ABC
Incidence angle	30°, 60°, 90°
Fault resistance	1 Ω , 50 Ω , 100 Ω
Sampling rate	200 kHz, 1 MHz, 5 MHz
SNR	50 dB

ues are employed to observe the behavior of the proposed approach in the presence of high noise levels in the analyzed signal. The success rate for testing with noise is attributed to the proposed approach after processing the faulted voltage signal for fault location because it is capable of setting apart the relevant fault occurrence characteristics from the noise associated and identifying the corresponding moment of arrival of the first TW and the successive reflections from the fault.

Based on the conditions above, in this paper, a SNR of 50 dB was added to the input signals across all scenarios. For the specific case of fault in 50% of the total line length, with an incidence angle of 60°, a fault resistance of 100 Ω , 1 MHz

of sampling rate, the SNR values of 30 dB, 40 dB, 50 dB, and 75 dB were used. The chosen SNR values were inspired by values found in the literature used in this subject of fault location [10, 13, 23].

The simulation of the power system was carried out using the alternative transients program (ATP) software, using the J. Marti's TL model, which is very accurate for transposed lines [24]. The transmission line was modeled using the line and cable constants (LCC) block, considering an ideally transposed transmission line, the skin effect, and the auto bundling. The wave speed was obtained through the LCC block. For a frequency of 1 kHz, the wave speed of the aerial mode was obtained as 295,966 km/s. The frequency at which the transformation matrix is calculated was 1 kHz, and the steady-state frequency was 50 Hz. The MATLAB[®] software was used to perform the single-ended and double-ended FL algorithms for extracting the TW arrival times. The signals studied for analysis have a duration of 100 ms (for five cycles of 20 ms). The available data window is 40 ms for pre-fault and 60 ms after fault occurrence. The techniques applied use one cycle after the fault incidence for fault location analysis.

4.3 Proposed methodology for fault location

The proposed approach in this paper involves 3 steps to estimate the fault location: detection, classification, and estimation of the distance from the fault occurrence to the analyzed terminal.

- Fault detection is the process of monitoring the current signals obtained at the terminal during system operation. These signals are compared with a predefined threshold characteristic of a healthy system.
- Fault classification identifies the fault type that has occurred. This result is crucial to provide the right faulted phase(s) for the signal processing in the next step.
- Fault location is carried out using the received faulted voltage signals. These signals are applied to the signal processing stage based on the studied approaches. The first arrived TW and the successive reflection from the fault are identified from the instants corresponding to the maximum values from the IMF1 (for SEEMD and DEEMD) or from the TEO (for SEEMDT and DEEMDT), and these instants are then used to estimate the fault location for both single-end and double-end measurements.

Detection is performed by analyzing the current signals received at terminal M, starting from the third cycle time (40 ms).

The fault index (FI) was proposed for detecting the faulted phase. The detection of the faulted phase is performed by comparing the maximum absolute value found in the current

Table 5 Mode transient state for each fault type

Fault type	Mode		
	Zero	α	β
AG	X	X	
BG	X	X	X
CG	X	X	X
ABG	X	X	X
BCG	X		X
ACG	X	X	X
AB		X	X
BC			X
AC		X	X
ABC		X	X

signal of the analyzed phase with the pre-fault index, when the system is healthy (FI_h), multiplied by a constant defined as the minimum threshold value.

The definition of the multiplier associated with FI_h was derived from the concept of rule based decision tree [25]. It is noted that different fault types can be identified by applying decision rules that use threshold values derived from the proposed fault index. To specify the FI, the magnitude of the maximum value found in each vector of the faulted current phases was identified and evaluated according to the fault type they represented.

After the tests, it was observed that the threshold associated with the healthy state of the system, for all fault types, was 135%. Thus, a single multiplier was used in the algorithm to detect the presence of a fault in a particular phase, achieving a success rate of 100% in all analyzed scenarios.

For the fault classification and location, the Clarke transformation was used to analyze the current and voltage signals characteristic data. Equation (8) defines the Clarke components of the phase currents, and they are analogous for the phase voltages [26].

$$\begin{bmatrix} I_\alpha \\ I_\beta \\ I_0 \end{bmatrix} = \frac{1}{3} \cdot \begin{bmatrix} 2 & -1 & -1 \\ 0 & \sqrt{3} & -\sqrt{3} \\ 1 & 1 & 1 \end{bmatrix} \cdot \begin{bmatrix} I_A \\ I_B \\ I_C \end{bmatrix} \quad (8)$$

Ideally, the α and β modes should show the transient state for all fault types, while the zero mode should be sensibitized only on faults involving ground. However, in the phase analysis, for example, the fault transient is not seen in the V_β on the AG fault. In contrast, in BC and BCG faults, the V_α mode does not contain a transient state when the fault occurs. Due to this, the proposed algorithm uses the sum of the V_α and V_β . Thus, the fault locator has better accuracy for all fault types. Table 5 can better illustrate in which mode the transient state is visible for each fault type [10].

The estimation of the distance from the fault occurrence to the analyzed terminal is found, using the TW single-ended

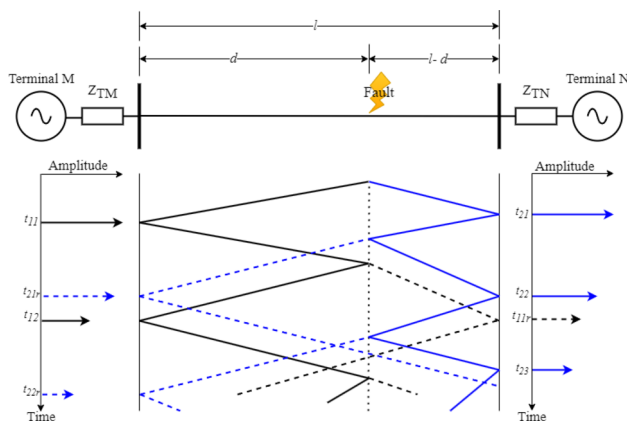


Fig. 3 Lattice diagram

or double-ended theory by (9) and (10), respectively [27, 28].

$$d = \frac{(t_b - t_f) \cdot v}{2} \quad (9)$$

$$d = \frac{l + (t_{11} - t_{21}) \cdot v}{2} \quad (10)$$

where t_f is the instant when the first TW arrives at the analyzed terminal, given in seconds; t_b is the instant when the successive reflection from the fault arrives at the analyzed terminal, given in seconds; v is the TW speed; l is the length of the transmission line, t_{11} is the instant when the first generated wave arrives at terminal M, given in seconds; t_{21} is the instant when the first generated wave arrives at terminal N, given in seconds. Figure 3 illustrates the Lattice diagram with the TWs arriving at the terminals.

Figure 4 presents the steps adopted for the methodology used by EMDT for FL using TW theory for the studied system, and the following procedure is performed:

1. The simulation of the studied test system is performed in the ATP software with the incidence angle, fault resistance, and fault occurrence location defined;
2. In the MATLAB[®] software, the algorithm is initiated by applying the SNR to the voltage and current signals obtained from the terminals to start the fault location process.
3. Detection (blocks 2 and 3 in Fig. 4): The pre-fault index, when the system is healthy (FI_h), is identified by the maximum absolute value found of the current signal in that period and a new one in the fault window is defined from analyzing the occurrence. At the time of the fault, the maximum absolute value of each phase is analyzed, and at the moment equivalent to the peak of the current signal, the index of this location is identified and called the fault index (FI);
4. Given the FI identification, this value is compared with 135% of the FI_h. If the FI value is above 1.35xFI_h, the

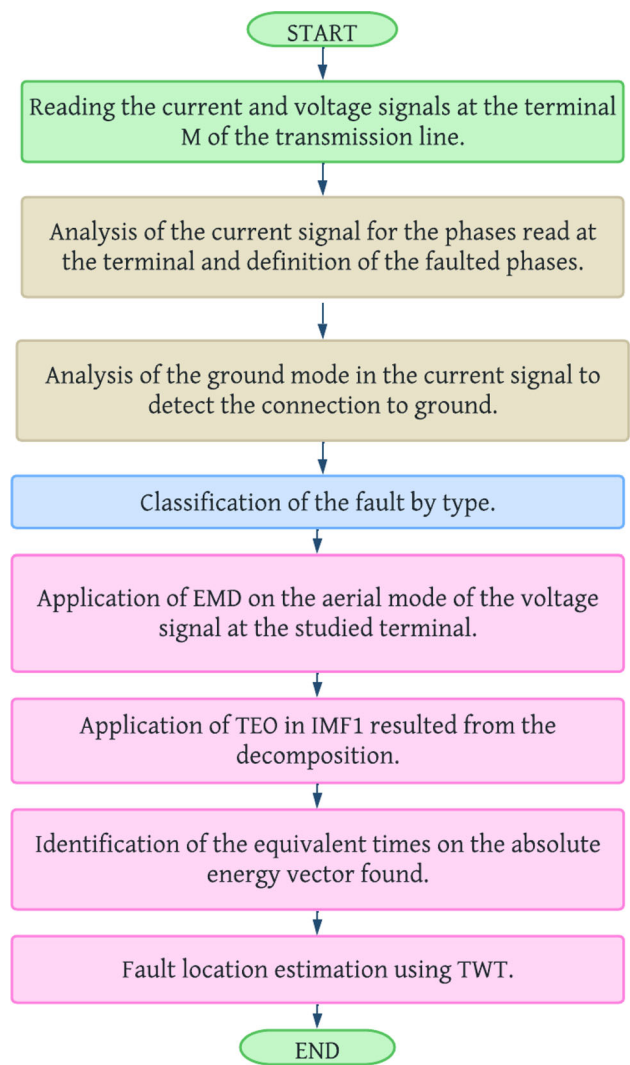


Fig. 4 Applied methodology for fault location

phase is under fault. Otherwise, the phase is healthy. The percentage value of 135% was the detection threshold defined by the authors from the amplitude of the measured signal compared to the signal without fault for all analyzed scenarios [29, 30];

5. The aerial mode of the current and voltage signals are determined at the terminals of the transmission line;
6. Classification (block 4 in Fig. 4): After the faulted phases are detected, the classification process is carried out by identifying the faulted phases and analyzing ground mode in the current signal to verify the presence of ground. The faulted current signals are classified according to their fault type;
7. Location (blocks 5-8 in Fig. 4): To estimate the FL, the V_α and V_β from the voltage signal are summed and the resulting value is applied in the empirical mode decomposition technique [10];

8. The decomposition in IMFs by EMD is performed, and the IMF1 (which is the first level of the intrinsic mode function) is chosen due to its better resolution;
9. TEO is used to visualize specific points on the signal [12, 13]. In this case, the TEO is applied to the IMF1 vector;
10. The first arrived TW and the successive reflection from the fault are identified from the instants corresponding to the maximum values of the absolute energy vector found at each terminal;
11. Fault location estimation using TW single-ended or double-ended theory by (9) and (10), respectively.
12. The percentage error is calculated. The value is found between the estimated distance and the theoretical distance, divided by the total line length, as presented in [2].

5 Case study

Traveling wave theory is used to locate the simulated faults. The voltage signal is processed after the classification process with EMDT to identify the TW's arrival times at the terminal. The results are compared with the standard approaches from the EMD to prove the influence of the TEO on accuracy [29, 31].

In total, 5400 fault cases were analyzed considering the 2 characteristic data extraction techniques (EMDT, and EMD) and their single-ended and double-ended approaches from the voltage signals on the terminal for the 1350 scenarios generated by the variation in the FL, the sampling rate, the fault resistance (R_F), and the incidence angle for all types of fault under consideration.

To demonstrate the behavior analyzed in each scenario, Figs. 5 and 6 illustrate a single-phase fault (AG) that was applied at $t = 0.043$ s, considering an incidence angle of 60° , $R_F = 100 \Omega$, at 50% of the total length of the TL. Figure 5 shows the EMD of the added V_α and V_β from the aerial mode of the faulted phase voltage signal with the sampling rate of 1 MHz in terminal M. The same analysis is done on terminal N. Figure 6 presents the application of TEO for the IMF1 from EMD on terminals M and N. The analysis considers a single-phase fault (AG). This type of fault and fault occurrence were chosen due to the high incidence of single-phase faults in the electrical power system, about 78%, and because the incidence is further away from the first reading terminal [2].

The instants corresponding to the maximum amplitudes in Fig. 6 represent the arrival times of the TW at each terminal. After the identification of these instants, the values are applied in (9) or in (10), depending on the studied approach (SE or DE). The estimation of the FL performed with SEEMDT and DEEMDT resulted in a percentage error of 0.03351% (121 m from the theoretical location) and 0.0104% (376 m from the theoretical location), respectively.

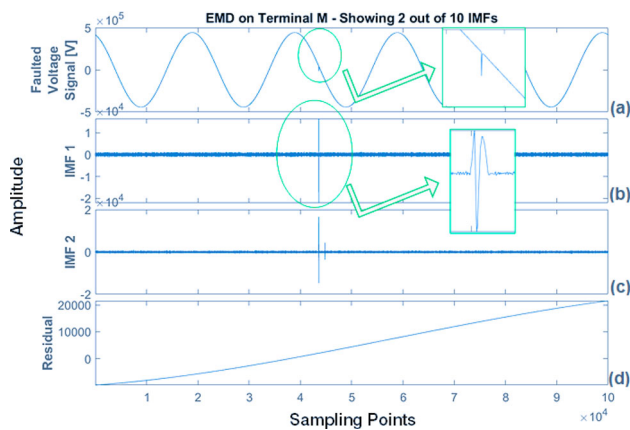


Fig. 5 EMD from AG fault read at terminal M for a sampling rate of 1 MHz

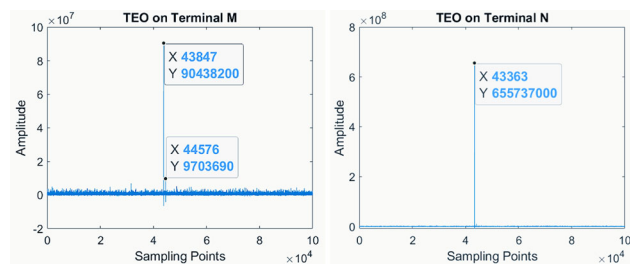


Fig. 6 TEO applied to IMF1 from EMD on both terminals

6 Sensitivity analysis

6.1 The effect of fault resistance and incidence angle

Table 6 presents the percentage error considering an AG fault, with FL at 70% of the TL, for all the sampling rates, the incidence angles, fault resistances, and the studied approaches (SEEMD, DEEMD, SEEMDT, and DEEMDT). The choice of 70% of the TL is due to its strategic location, which is a local with an intermediate difficulty for fault location estimation to observe the efficiency of the approaches applied. Fault resistance variations in the range of 1Ω – 100Ω do not have a significant effect on FL results using the proposed algorithms, except in some situations in $R_F = 50 \Omega$, that show the highest error values.

In general, the results show that the best accuracy depends on the technique applied for signal analysis (the best results are with approaches using the TEO). As confirmed in the literature, the TW theory has proved to be immune to fault resistance and fault incidence angle for the values adopted in this study [2]. The DEEMDT presented the best results in most of the scenarios and lower variation among the fault resistances and incidence angles.

Table 6 Percentage error for AG fault with all approaches applied

Sampling rate	Incidence angle	Technique	Fault resistance		
			1 Ω	50 Ω	100 Ω
200 kHz	30°	SEEMD	8.830	30.4326	9.036
		DEEMD	7.052	58.434	0.680
		SEEMDT	0.198	0.008	0.008
		DEEMDT	0.142	0.063	0.063
	60°	SEEMD	2.269	0.830	12.134
		DEEMD	11.652	11.162	4.458
		SEEMDT	0.008	0.198	0.198
		DEEMDT	0.063	0.063	0.063
	90°	SEEMD	10.680	6.569	9.462
		DEEMD	11.162	0.474	7.952
		SEEMDT	2.8850	8.419	2.870
		DEEMDT	0.063	0.063	0.348
1 MHz	30°	SEEMD	29.589	24.327	27.986
		DEEMD	16.790	7.829	1.622
		SEEMDT	0.034	0.198	0.239
		DEEMDT	0.146	0.015	0.105
	60°	SEEMD	9.668	2.212	8.707
		DEEMD	0.351	5.202	1.210
		SEEMDT	0.239	0.116	0.116
		DEEMDT	0.146	0.104	0.104
	90°	SEEMD	13.968	11.928	9.488
		DEEMD	23.412	15.930	17.945
		SEEMDT	6.667	1.3487	1.899
		DEEMDT	0.104	0.063	0.063
5 MHz	30°	SEEMD	0.494	2.211	4.794
		DEEMD	13.908	24.406	12.231
		SEEMDT	0.190	56.6934	33.674
		DEEMDT	0.146	0.146	0.137
	60°	SEEMD	26.415	24.212	17.421
		DEEMD	32.192	58.106	30.877
		SEEMDT	5.162	3.872	9.446
		DEEMDT	0.137	0.137	0.121
	90°	SEEMD	12.127	14.125	15.481
		DEEMD	9.304	5.095	15.881
		SEEMDT	3.7411	1.949	3.741
		DEEMDT	12.921	63.594	12.922

6.2 The effect of fault type

Figures 7 and 8 present the average percentage error using the sampling rates of 200 kHz, 1 MHz, and 5 MHz for voltage-faulted signals, respectively. The SEEMD, DEEMD, SEEMDT, and DEEMDT were applied in all types of faults, every fault location presented in Table 4 of the TL extension, with an incidence angle at 60°, and a fault resistance of 100 Ω .

Using DEEMDT, the results are generally the best for all fault types and Figs. 7 and 8 show it. Figure 7 shows that, for all sampling rates used, the behavior is similar for all fault types and the lowest values found are using DEEMDT with a sampling rate of 5 MHz. Figure 8 shows the influence of fault type for the techniques SEEMDT, SEEMD, and DEEMD. The best results are for AG with SEEMDT, regardless of the sampling rate, and the worst results are using the standard EMD technique, proving the superior performance when using TEO.

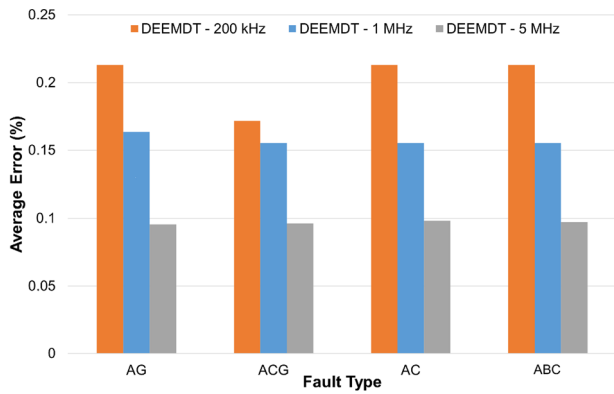


Fig. 7 Average error for all fault types applied to DEEMDT

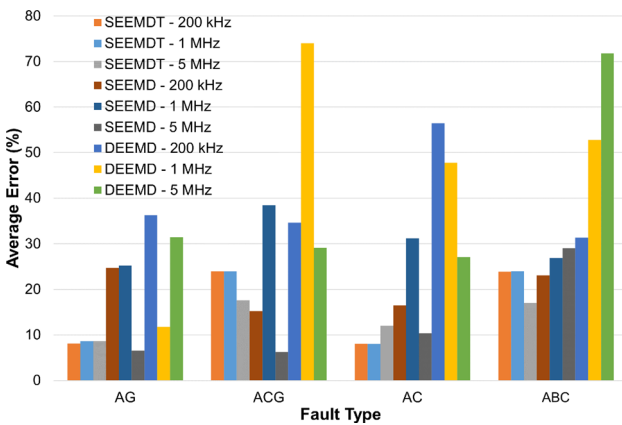


Fig. 8 Average error for all fault types applied to SEEMDT, DEEMD, and SEEMDT

6.3 The effect of sampling rate

The TW real devices accuracy essentially depends on the high sampling rate and they can already be found in the market with sampling rates varying from 1 to 5 MHz. Some intelligent electronic devices manufacturers have indicated plans to implement 10 MHz sampling rates in the near future [32–

37]. Table 7 presents a comparison of applications (market available devices and the methodology studied in this work) that use the traveling wave theory with high sampling rates.

Hence, this section aims to present the analysis of the techniques used in this work for different sampling rates and to present its influence on the accuracy of TW-based FL. Table 8 presents the total average percentage error for the techniques analyzed in this work, considering occurrences of AG faults in the TL extension, the incidence angle of 60°, and different sampling rates (200 kHz, 1 MHz, and 5 MHz).

In this analysis, it is observed that the DEEMDT presents the smallest total average percentage error for all variations in the sampling rate and the fault resistances. The best accuracy is found at 5 MHz, and with this sampling rate it was easier to estimate the FL in a larger number of samples of the analyzed universe. Figure 9 shows the results of DEEMDT for a single-phase fault (AG), all the incidence angles, with $R_F = 100 \Omega$, on the entire TL extension, and the studied sampling rates. The behavior throughout the TL was as expected, with the typical V shape and the central minimum, except for the incidence angle of 90°, the sampling rate of 5 MHz, at FLs of 50% and 70% of the total line length, where the percentage errors are higher than 10%. With the behavior presented, it is possible to observe the independence of the DEEMDT from the variables changed.

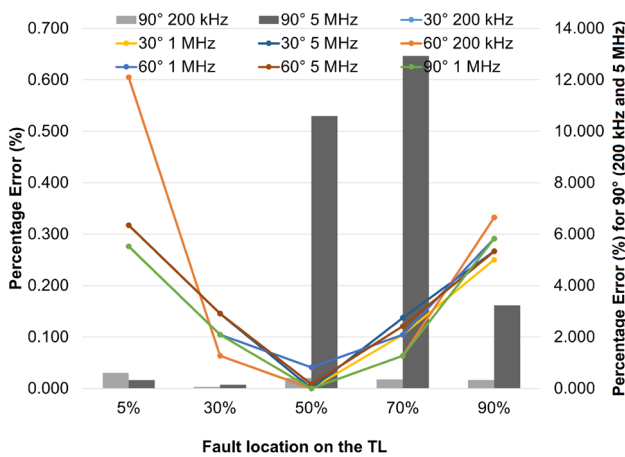
A suggested optimal sampling rate is observed from Table 6, with the individual results and behaviors for the single-phase (AG) fault, with fault location at 70% of the transmission line (an intermediate difficulty for fault estimation according to Fig. 9), considering the variation in R_F , the angle of incidence, and the sampling rate for all applied approaches. It is observed that with a sampling rate of 200 kHz, the approaches that use EMDT provide greater accuracy and independence from the variables under observation, such as R_F and angle of incidence. This behavior was also observed by the authors in the analysis of a transmission line with different characteristics [29]. For sampling rates of 1

Table 7 Summary of available devices in the market and comparison with the method proposed in this work

Application	Sampling rate	FL method	Performance
SEL-411 L	1.5625 MHz	Double-ended	High computational cost due to high-frequency analysis and complex algorithms
GE RPV311	5 MHz	Single-ended	Moderate computational cost for high precision recording and transient, analysis
SEL-T400L	1 MHz	Double-ended	Very high computational cost due to high-speed sampling and real-time processing
This work	200 kHz, 1 MHz, and 5 MHz	Single-ended/ Double-ended	Low computational cost for simulations in MATLAB®. Methodology not commercial yet

Table 8 Percentage error for different sampling rates for an AG fault

R_F	Sampling rate	SEEMD	DEEMD	SEEMDT	DEEMDT
1 Ω	5 MHz	8.658772	18.43762	23.87541	0.096298
	1 MHz	28.76024	21.19967	7.975265	0.16347
	200 kHz	19.21168	37.51204	1.197428	0.12106
50 Ω	5 MHz	10.66923	12.23001	26.57213	0.098135
	1 MHz	12.51507	37.37972	26.92696	0.163474
	200 kHz	6.569733	16.69153	4.2647	0.212875
100 Ω	5 MHz	6.543453	31.45554	8.611373	0.095396
	1 MHz	25.22519	11.76763	8.560645	0.163505
	200 kHz	24.71991	36.21245	8.068809	0.212875

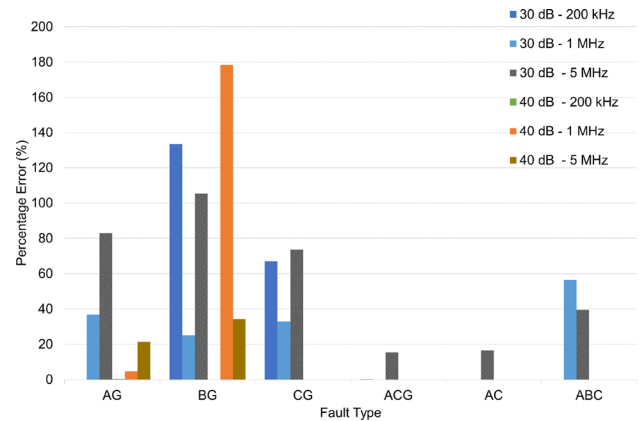
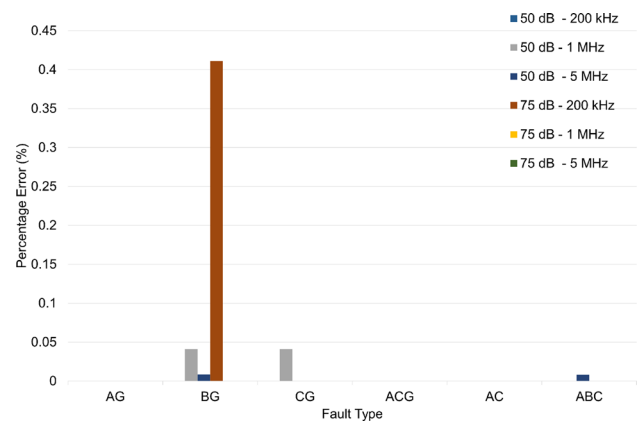
**Fig. 9** Percentage error along the entire length of the TL for DEEMDT

MHz and 5 MHz, the highest accuracy is regardless of the R_F at 90° and 60° , respectively.

6.4 The effect of SNR

Figures 10 and 11 present the SNRs of 30 dB, 40 dB, 50 dB, and 75 dB applied to all sampling rates and fault types for 50% of the total line length, with an incidence angle of 60° , a fault resistance of 100 Ω , and for the DEEMDT technique.

From the results obtained, it is observed that for noisier signals associated with the voltage signal for FL, at 30 dB and 40 dB (Fig. 10), the difficulty of fault estimation increases for some of the fault types. Such analysis confirms the limitation of the EMD, even associated with TEO, in the face of higher noise superimposed on the signals analysis. The sampling rate of 200 kHz showed better accuracy with noisier signals, while the sampling rates of 1 MHz and 5 MHz presented smaller errors for the SNR of 50 dB and 75 dB (Fig. 11). The largest error was 0.4% for the single-phase BG with sampling rate of 200 kHz.

**Fig. 10** SNR analysis for all fault types with 30 dB and 40 dB**Fig. 11** SNR analysis for all fault types with 50 dB and 75 dB

6.5 Analysis of computational cost

The platform used for the simulations has a 64-bit operating system, with an AMD Ryzen 7 4800H processor, with Radeon Graphics (2.90 GHz), 8 GB of RAM, and 512 GB of ROM on SSD.

Considering that the majority of the computational cost refers to the processing of the EMD application in the voltage signal, the required time for fault location is dependent

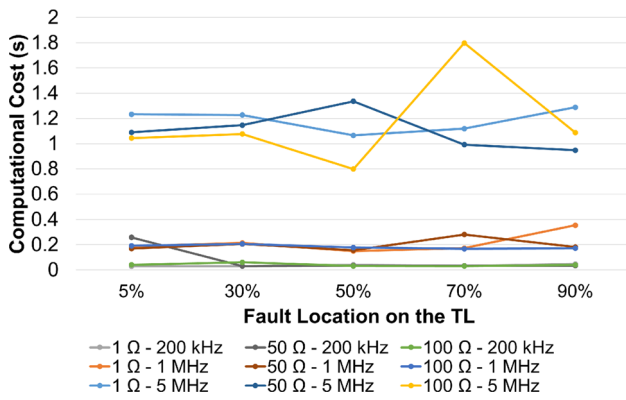


Fig. 12 Computational cost along the entire length of the TL for DEEMDT

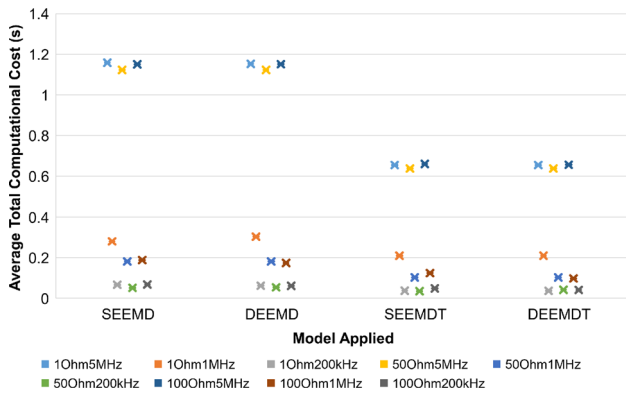


Fig. 13 Average total computational cost for FL with EMD approaches

on the sampling rate, the fault resistance, and the fault location, and independent from the variation in the fault type and the incidence angle. Thus, Fig. 12 presents the computational cost for the single-phase fault along the entire length of the TL, with an incidence angle of 90°, and for all applied R_F and sampling rates. It is observed that the highest computational cost for fault location is at 5 MHz, with an average value of 1.150 s considering all the fault locations along the line, followed by 0.199 s for 1 MHz, and 0.052 s for 200 kHz.

Figure 13 presents the average total computational cost for all incidence angles, fault resistances, sampling rates studied, for all FL, and the approaches adopted to extract the characteristic data from the aerial mode of faulted voltage signals. From the results obtained, it is observed that: the computational cost is dependent on the sampling rate for the EMD approaches, but the difference in timings between the sampling rates of 200 kHz and 1 MHz is minimal; for each studied sampling rate, the computational cost is similar for different studied incidence angles; approaches using TEO, in general, have lower computational cost; the average total computational cost for the approaches and variables studied is 0.505 s for SEEMD, 0.506 s for DEEMD, 0.295 s for SEEMDT, and 0.294 s for DEEMDT.

7 Conclusions

This paper presented a method of fault location using the single-ended and the double-ended TW theory and EMDT to extract characteristic data from voltage signals in their aerial mode to estimate the distance from terminals to the fault position in the AC transmission line.

By analyzing 5400 fault cases, it was confirmed that faults were accurately detected and classified with a 100% success rate. This outcome serves as evidence of the effectiveness of employing the defined detection threshold, and it demonstrated satisfactory location error rates for the EMDT approach based on TW.

The numerical and graphical results prove that the proposed methodology (EMDT) can extract the characteristic data of the voltage signals and estimate the FL with high accuracy for single- and double-ended analysis. The results are compared with the standard approaches from the EMD to prove the influence of the TEO on accuracy. According to the results shown in Tables 6 and 8, the FL is affected when TEO is not used, being more sensitive to variation in fault resistance and sampling rate.

The SEEMDT and DEEMDT applied to faulted voltage signals considering the presence of noise demonstrated the best results regardless of the fault incidence angle, fault resistance, and sampling rate. The average accuracy in Table 6 for the single-phase fault, the most common fault type in transmission lines, was 95.47% and 99.89%, at 200 kHz, and 97.44% and 99.90%, at 1 MHz, for SEEMDT and DEEMDT, respectively. The EMDT showed lower accuracy to the higher sampling frequency, 5 MHz, with values of 92.00% and 96.59% for SEEMDT and DEEMDT, respectively. The results justify the theory of how the EMD technique is known for limitations in noisy signals and higher sampling rates [38].

To implement devices using the methodology proposed in this paper, various hardware and software components are required, such as intelligent protection relays, digital signal processors, monitoring and control systems, and supporting infrastructure. Given the proposal for high-speed signal processing and complex real-time calculations, advanced processing hardware and high capacity memory are necessary to handle the high data rate and the need for rapid responses. As devices that use traveling wave theory and high sampling rates, similar to those cited in the paper, have been commercialized for real-time protection systems, the authors believe in the feasibility of implementing the proposed methodology in fault locators.

For future work, the authors plan to improve the methodology applied in order to upgrade the accuracy for fault location with noisy signals and higher sampling rates since there are devices with sampling frequencies in the MHz range. Additionally, an exploration of the proposed approach is applied for cross-country faults and evolving faults using

the sampling rates from this paper (200 kHz, 1 MHz, and 5 MHz) [39, 40], and the impact of measurement errors on the proposed method's accuracy is planned. The authors shall consider the presence of the instrument transformers since their dynamic behavior for high-frequency transients may have an important influence on FL accuracy. Nonetheless, the results presented in this work are valid as a trend in accuracy for the different scenarios simulated.

Funding Funding was provided by Coordenação de Aperfeiçoamento de Pessoal de Nível Superior (Grant No. Financing Code 001).

References

- Stringfield T, Marihart D, Stevens R (1957) Fault Location Methods for Overhead Lines. *Trans Am Inst Electr Eng Part III Power Appar Syst* 76:518–529. <https://doi.org/10.1109/AIEEPAS.1957.4499601>
- Saha J, Rosolowski E (2010) Fault location on power networks. *Power Systems*
- Raza A, Benrabah A, Alquthami T, Akmal M (2020) A review of fault diagnosing methods in power transmission systems. *Appl Sci* 10(4):1312
- Panahi H, Zamani R, Sanaye-Pasand M, Mehrjerdi H (2021) Advances in transmission network fault location in modern power systems: review outlook and future works. *IEEE Access* 9:158599–158615
- Krzysztof G, Kowalik R, Rasolomampionona D, Anwar S (2011) Traveling wave fault location in power transmission systems: an overview. *J Electr Syst* 7:287–296 (9)
- Geethanjali M, Sathya priya K (2009) Combined wavelet transforms and neural network (WNN) based fault detection and classification in transmission lines. In: 2009 International conference on control, automation, communication and energy conservation. pp 1-7
- Akmaz D, Mamiç M, Arkan M, Tağluk M (2018) Transmission line fault location using traveling wave frequencies and extreme learning machine. *Electr Power Syst Res* 155:1–7
- Chan S, Oktavianti I, Puspita V, Nopphawan P (2019) Convolutional adversarial neural network (CANN) for fault diagnosis within a power system : addressing the challenge of event correlation for diagnosis by power disturbance monitoring equipment in a smart grid. In: 2019 International conference on information and communications technology (ICOIACT). pp 596-601
- Reis R, Lopes F, Ribeiro E, Moraes C, Silva K, Britto A, Agostinho R, Rodrigues M (2023) Traveling wave-based fault locators: performance analysis in series-compensated transmission lines. *Electr Power Syst Res* 223:109567
- Rezaei D, Gholipour M, Parvaresh F (2022) A single-ended traveling-wave-based fault location for a hybrid transmission line using detected arrival times and TW's polarity. *Electr Power Syst Res* 210:108058
- Gadanayak D, Mallick R (2019) Microgrid differential protection scheme using downsampling empirical mode decomposition and Teager energy operator. *Electr Power Syst Res* 173:173–182. <https://doi.org/10.1016/j.epsr.2019.04.022>
- Ge M, Gao H, Liu Z, Yu D (2019) Fault location of UHV DC transmission line based on variational mode decomposition and energy operator. In: 2019 IEEE 8th International conference on advanced power system automation and protection (APAP). pp 616-620
- Huai Q, Liu K, Hooshyar A, Ding H, Chen K, Liang Q (2021) Single-ended line fault location method for multi-terminal HVDC system based on optimized variational mode decomposition. *Electr Power Syst Res* 194:107054. <https://doi.org/10.1016/j.epsr.2021.107054>
- Shi L, Hui J, Zhang W, Xue A, Jiang E (2022) Fault diagnosis of transmission lines based on improved complete ensemble empirical mode decomposition. In: 2022 6th International conference on power and energy engineering (ICPEE). pp 158-162
- Liguo Z, Xu H, Jian J, Tianye G, Yongsheng M (2009) Power systems faults location with traveling wave based on Hilbert-Huang transform. In: 2009 International conference on energy and environment technology. vol 2 pp 197-200. <https://doi.org/10.1109/ICEET.2009.285>
- Aggarwal A, Malik H, Sharma R (2016) Feature extraction using EMD and classification through probabilistic neural network for fault diagnosis of transmission line. In: 2016 IEEE 1st International conference on power electronics, intelligent control and energy systems (ICPEICES). pp 1-6 <https://doi.org/10.1109/ICPEICES.2016.7853709>
- Huang N, Shen Z, Long S, Wu M, Shih H, Zheng Q, Yen N, Tung C, Liu H (1998) The empirical mode decomposition and the Hilbert spectrum for nonlinear and non-stationary time series analysis. *Proc R Soc London Series A Math Phys Eng Sci* 454:1471–2946. <https://doi.org/10.1098/rspa.1998.0193>. (3)
- Rilling G, Flandrin P, Gonçalves P (2003) On, empirical mode decomposition and its algorithms. *EURASIP Workshop on nonlinear signal and image processing*. IEEE, Grado, Italy
- Braz V, Souza A, Araújo L, Rodrigues G (2017) Estudo da decomposição em modos empíricos e sua aplicação em sinais não estacionários. XXXV Simpósio Brasileiro de Telecomunicações e Processamento de Sinais (SBrT2017). <https://doi.org/10.14209/sbrt.2017.113>. (in Portuguese)
- Kaiser J (1993) Some useful properties of Teager's energy operators. In: IEEE International conference on acoustics, speech, and signal processing. 3:149–152. <https://doi.org/10.1109/ICASSP.1993.319457>
- Gashimov A, Babayeva A, Nayir A (2009) Transmission line transposition. In: 2009 International conference on electrical and electronics engineering - ELECO 2009. pp 1-364-I-367
- IEEE Recommended practice for monitoring electric power quality. *IEEE Std 1159-2019 (Revision of IEEE Std 1159-2009)*. pp 1-98 (2019). <https://doi.org/10.1109/IEEESTD.2019.8796486>
- Zeng R, Wu Q, Zhang L (2022) Two-terminal traveling wave fault location based on successive variational mode decomposition and frequency-dependent propagation velocity. *Electr Power Syst Res* 213:108768
- Marti J (1982) Accurate Modelling of Frequency-Dependent Transmission Lines in Electromagnetic Transient Simulations. *IEEE Trans Power Appar Syst PAS*–101:147–157
- Singh B, Mahela O, Manglani T (2018) Detection and classification of transmission line faults using empirical mode decomposition and rule based decision tree based algorithm. In: 2018 IEEE 8th Power India international conference (PIICON). pp 1-6 <https://doi.org/10.1109/POWERI.2018.8704372>
- Schweitzer E, Guzmán A, Mynam M, Skendzic V, Kasztenny B, Marx S (2014) Locating faults by the traveling waves they launch. In: 2014 67th Annual conference for protective relay engineers. pp 95-110
- Bewley L (1931) Traveling waves on transmission systems. *Trans Am Inst Electr Eng* 50(2):532–550
- Gale P, Crossley P, Bingyin X, Yaozhong G, Cory B, Barker J (1993) Fault location based on travelling waves. In: 1993 Fifth international conference on developments in power system protection. pp 54-59
- Oliveira A, Moreira F, Picanço A (2023) Accuracy analysis using the EMD and VMD for two-terminal transmission line fault

- location based on traveling wave theory. *Electr Power Syst Res* 224:109667
30. Oliveira A, Moreira F, Picanço A (2022) Application of Hilbert-Huang and Stockwell transforms to fault location in transmission lines using traveling wave theory. In: 2022 IEEE 7th International energy conference (ENERGYCON). pp 1-6 <https://doi.org/10.1109/ENERGYCON53164.2022.9830381>
 31. Zhang Q, Ma W, Li G, Ding J, Xie M (2022) Fault diagnosis of power grid based on variational mode decomposition and convolutional neural network. *Electr Power Syst Res* 208:107871. <https://doi.org/10.1016/j.epsr.2022.107871>
 32. Laboratories S (2022) Advanced line differential protection, automation, and control system. <https://selinc.com/products/411L/>
 33. Electric G (2022) Reason RPV311 digital recorder w/ PMU and TWFL. <https://862d.short.gy/GE-RPV311>
 34. Laboratories S (2022) Time-domain line protection. <https://selinc.com/products/T400L/>
 35. ERLPhase Power technologies. L-PRO 2100 Multi-function transmission line protection relay, <https://www.erlphase.com/downloads/>
 36. Hitachi Energy RED670 - Transmission line differential protection, <https://www.hitachienergy.com/br/pt/products-and-solutions/>
 37. Lopes F, Reis R, Silva K, Martins-Britto A, Ribeiro E, Moraes C, Rodrigues M (2021) Past, present, and future trends of traveling wave-based fault location solutions. 2021 Workshop on communication networks and power systems (WCNPS). pp 1-6
 38. Dragomiretskiy K, Zosso D (2014) Variational mode decomposition. *IEEE Trans Signal Process* 62:531–544
 39. Biswal S, Biswal M, Malik O (2018) Hilbert Huang transform based online differential relay algorithm for a shunt-compensated transmission line. *IEEE Trans Power Deliv* 33:2803–2811
 40. Prasad C, Biswal M (2020) Time-domain current information based faulty phase detection in thyristor controlled series compensated transmission system. In: 2020 International conference on power, instrumentation, control and computing (PICC). pp 1-5

Publisher's Note Springer Nature remains neutral with regard to jurisdictional claims in published maps and institutional affiliations.

Springer Nature or its licensor (e.g. a society or other partner) holds exclusive rights to this article under a publishing agreement with the author(s) or other rightsholder(s); author self-archiving of the accepted manuscript version of this article is solely governed by the terms of such publishing agreement and applicable law.